Available online at www.sciencedirect.com
SCIENCE DIRECT
Journal of Asian Earth Sciences 26 (2006) 461–476
Journal of Asian Earth Sciences
www.elsevier.com/locate/jaes

Characteristics of ophiolite-related metamorphic rocks in the Beysehir ophiolitic mélange (Central Taurides, Turkey), deduced from whole rock and mineral chemistry

Ömer Faruk Çelik[a,*], Michel F. Delaloye[b]

[a]Department of Geology, Kocaeli University, İzmit/Kocaeli 41150, Turkey
[b]Department of Mineralogy, University of Geneva, 1205 Geneva 4, Switzerland

Received 2 December 2003; accepted 21 October 2004

Abstract

Small outcrops of the metamorphic rocks of the Beysehir ophiolite appear to the west of Gencek and to the south of Durak (South of Beysehir Lake) in the Central Tauride Belt in Turkey. Amphibolitic rocks in the ophiolitic mélange have an igneous origin. Protoliths of these rocks were probably alkali basalts, gabbros or some ultramafic cumulates, such as pyroxenite. The amphibolites of the Beysehir Ophiolite can be divided into four groups: (1) amphibole + garnet + plagioclase ± epidote (as secondary minerals) ± opaque such as ilmenite ± accessory minerals such as sphene and apatite; (2) amphibole + pyroxene + plagioclase ± epidote ± accessory minerals such as sphene, apatite ± chlorite, calcite (as secondary mineral); (3) amphibole ± plagioclase ± opaque ± accessory minerals; (4) amphibole + plagioclase ± epidote ± biotite and muscovite ± opaque ± accessory minerals. These metamorphic rocks show mainly granoblastic, granonematoblastic, porphyroblastic and/or poikiloblastic textures. All amphiboles in the amphibolites are calcic and cluster in the range from magnesio-hastingsite, pargasite to actinolite. Amphibole compositions are characterized by SiO_2 = (38.02–54.3%), Al_2O_3 = (1.5–12.8), FeO = (10.03–14.67%), K_2O = (0.2–1.8%), MgO = (5.5–15.7), Mg* = (0.3–0.8). The amphibolites show an alkaline to subalkaline character. However, the primitive mantle normalized incompatible trace element diagram shows close similarity with the typical ocean island basalt (OIB) pattern. The Rock/Chondrite normalized REE diagram of the amphibolites also confirms their OIB signature. Tectonomagmatic discrimination diagrams based on the immobile trace elements suggest a mostly within-plate alkali basalt (WPB) environment. Beysehir ophiolitic mélange contains amphibolites from ophiolite-related metamorphic rocks, but the matrix of the Beysehir ophiolitic mélange is not metamorphosed. Blocks of metamorphic rocks and the ophiolitic rocks may have been incorporated into the ophiolitic mélange in an oceanic environment during the Late Cretaceous by tectonic forces.

Keywords: Mineralogy and petrography; Geochemistry; Amphibolite; Hydrothermal alteration

1. Introduction

The Beysehir-Hoyran-Hadim Nappes located in the Central Tauride Belt of Turkey (Fig. 1), crop out over a distance of 700 km from NW to SE. They consist of Mesozoic carbonate platform, deep-sea and ophiolitic units that were thrust from a Northern Neotethyan ocean basin onto the Tauride carbonate platform to the south in latest Cretaceous time (Sengör and Yýlmaz, 1981; Tekeli, 1981; Robertson and Dixon, 1984; Stampfli, 2000; Andrew and Robertson, 2002).

Ricou et al. (1975) proposed that there were two major geological stages in the emplacement of the Beysehir ophiolite. During the first stage the Beysehir ophiolite formed a pile of nappes with the overlying units, which were emplaced during Upper Cretaceous time into a 'wildflysch' basin. Andrew and Robertson (2002) found that the 'wildflysch' is composed mainly of debris flow deposits. In the second stage, all the units were transported to their present position on the Tauride

* Corresponding author. Tel.: +90 262 335 1168; fax: +90 262 335 2812.
E-mail address: fcelik@kou.edu.tr (Ö.F. Çelik).

1367-9120/$ - see front matter © 2005 Elsevier Ltd. All rights reserved.
doi:10.1016/j.jseaes.2004.10.008

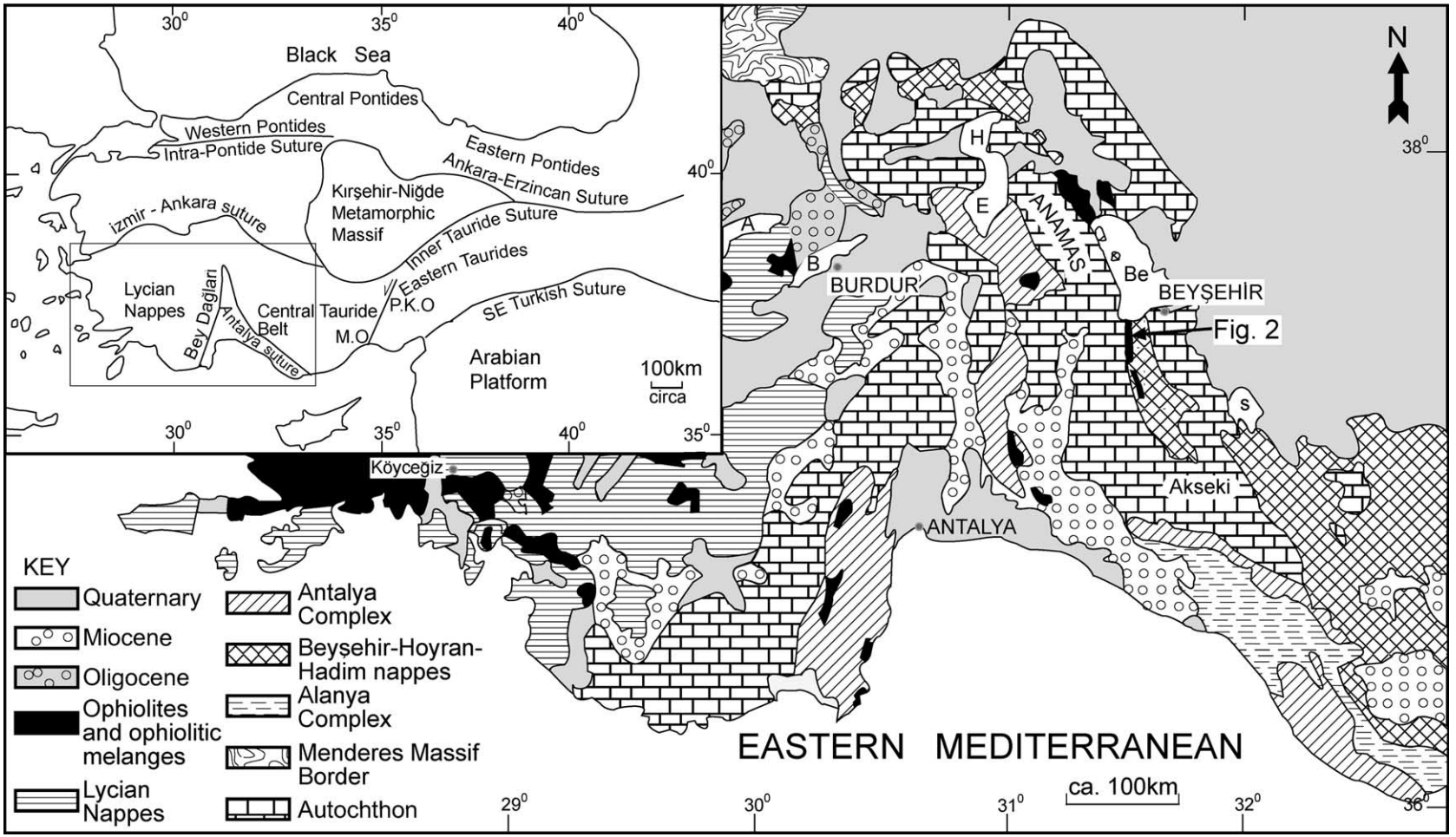

Fig. 1. Outline tectonic map of SW Turkey (modified from Gutnic et al., 1979; Andrew and Robertson, 2002; Vrielynck et al., 2003). A, Lake Acı; B, Lake Burdur; H, Lake Hoyran; E, Lake Egridir; Be, Lake Beysehir; S, Lake Sugla. Inset: main tectonic subdivisions of Turkey. M.O., Mersin Ophiolite; P.K.O., Pozantı-Karsantı Ophiolite.

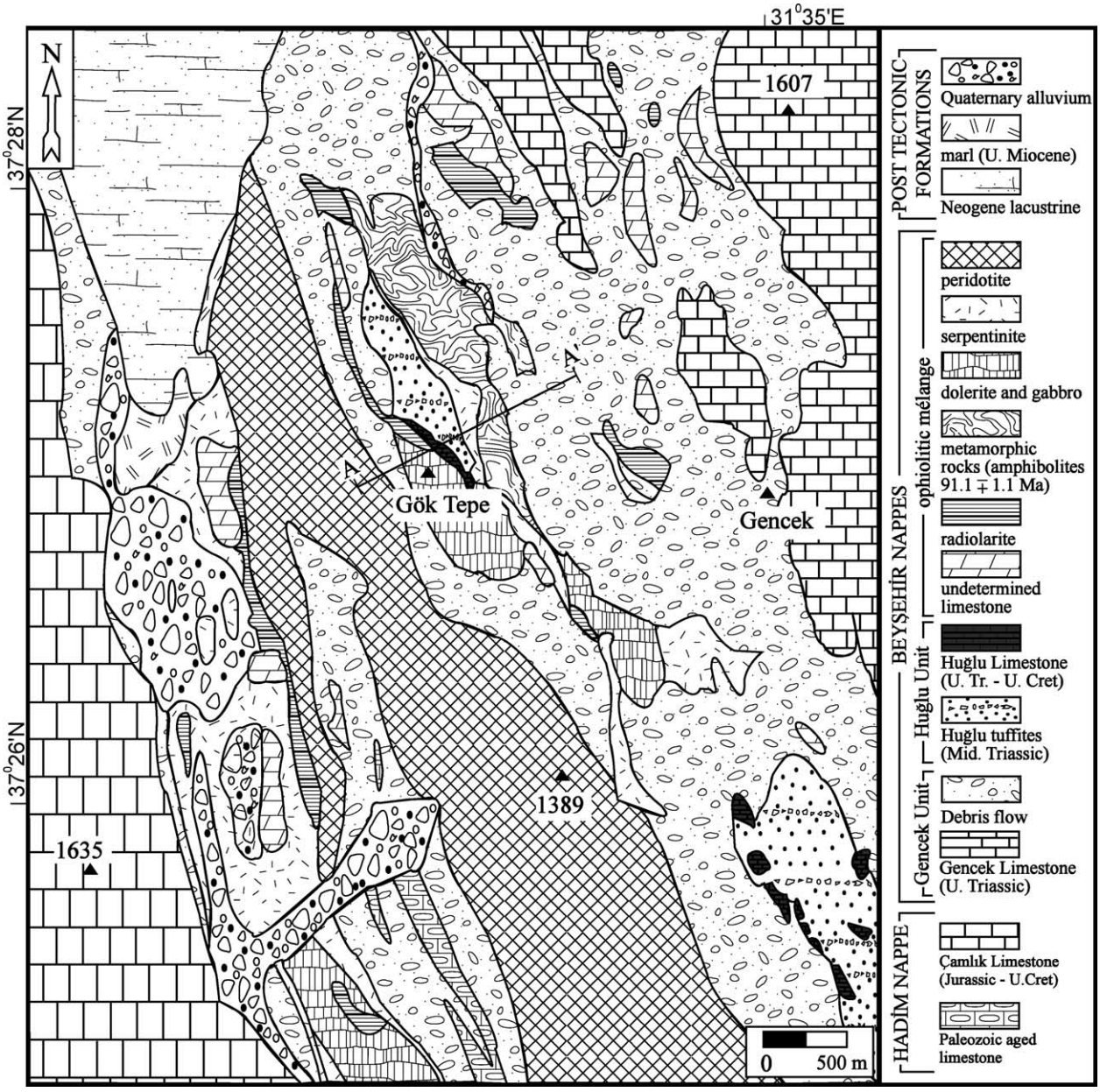

Fig. 2. Generalized geological map of the area south of Beysehir lake (modified from Monod, 1977).

carbonate platform during Lutetian time. Andrew and Robertson (2002) and Robertson (2002) suggested that subduction/ accretion processes were responsible for the emplacement of the Beysehir ophiolite and related units, which were emplaced southwards onto the northern edge of the Tauride carbonate platform during the latest Cretaceous, followed by final Eocene southward thrusting during or after continental collision. They also proposed that the uppermost Hadim Nappe is far-travelled, and was emplaced during Eocene thrusting.

The metamorphic rocks associated with the ophiolite have been studied in small outcrops located to the south of Durak (not shown in the geological map) and to the west of Gencek Village (Fig. 2). The metamorphic rocks in the region are amphibolites, garnet and/or pyroxene bearing amphibolite, which are tectonically bounded by serpentinites and debris flows (Fig. 3). Garnet-micaschist and quartzites are also reported by Monod (1977).

The aim is to discuss the origin and geodynamic environment of the metamorphic rocks and their geothermobarometric evolution utilising petrographical, mineralogical and geochemical study. Comparison of sole rocks from the western part of the Taurus Range (Lycian and Antalya ophiolites) as from its eastern part will contribute to the Neotethys closing history.

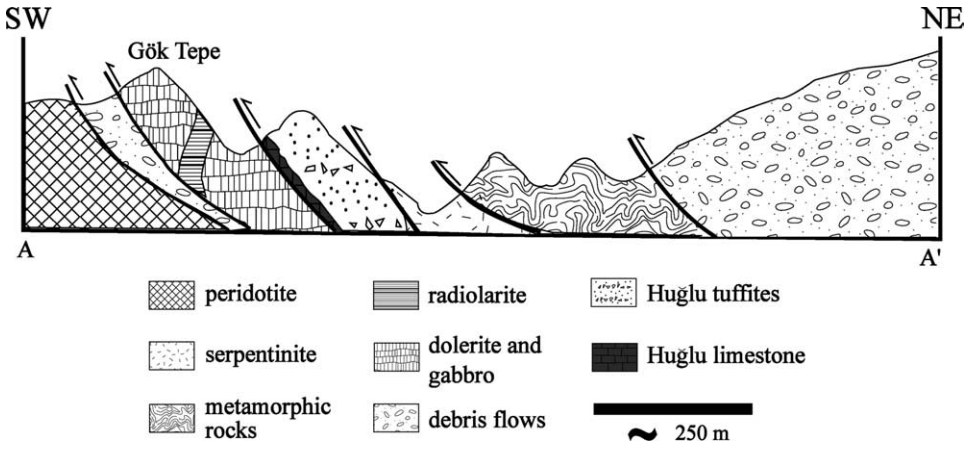

Fig. 3. Cross-section from west of Gencek showing the geological relationships of the metamorphic rocks.

2. Regional geological setting

There are four major tectonostratigraphic units of Late Paleozoic-Mesozoic age in the Beysehir-Hoyran-Hadim Nappes in the Beysehir area (Monod, 1977; Andrew and Robertson, 2002):

1. Bademli-Çamlik unit (Hadim Nappe) consisting mainly of Devonian-Carboniferous schists, quartzite, dolomite and Permian to Late Cretaceous limestones.
2. Upper Cretaceous ophiolite and ophiolitic mélange.
3. Boyali Tepe and Gencek units composed of Late Triassic to Late Cretaceous neritic-pelagic limestone, brecciated radiolarites, and volcanics. These two units occur as fragmentary blocks in a matrix which includes radiolarian chert, neritic limestone, pelagic limestone, calcarenite and detrital quartz.
4. Huglu unit, including Middle Triassic tuffites and volcanic breccias, Upper Triassic–Upper Cretaceous pelagic and cherty limestones.

Regionally these allochthonous units overlie a basement of Tauride platform carbonates.

Robertson and Dixon (1984) and Sengör et al. (1984) suggested that the Beysehir and Lycian Nappes (Fig. 1) could be restored to a position within the northern part of the Neotethys, although these two units differ from each other in terms of their lithology and age of final emplacement. The Beysehir nappes were finally emplaced in Late Eocene time (Özgül, 1984; Robertson, 2000; Andrew and Robertson, 2002), whereas the Lycian nappes were finally emplaced in Late Miocene time (Collins and Robertson, 1998).

The Beysehir Ophiolitic unit is located within synclines of the Beysehir-Hoyran Nappes as a huge thrust sheet or as dismembered thrust slices. Elitok (2001) reported that the ophiolitic unit to the north of Beysehir Lake consists of harzburgitic tectonites above, underlain by metamorphic sole rocks and ophiolitic melange below. The metamorphic sole rocks at the base of harzburgitic tectonites consist of amphibolite, gneissic amphibolite, amphibole schist, calc-schist and quartzite (Elitok, 2001). North of Beysehir Lake both the metamorphic sole rocks and the ophiolite are cut by numerous isolated tholeiitic dolerite dikes with chilled margins. These rocks have an arc-related chemical composition (Elitok, 2001).

Further west in the area studied, near Gencek (Fig. 2) the ophiolitic mélange consists of blocks of harzburgite, dunite, pyroxenite, amphibolite, neritic and pelagic limestone, radiolarian chert, basic volcanic rock, volcaniclastic sediment and serpentinite. The matrix of the ophiolitic mélange is ophiolite-derived sandstone and mudstone (Andrew and Robertson, 2002). A tectonic slice of cumulate gabbro near Çamlık, consisting of plagioclase ($An_{50–60}$), olivine, ortho- and monoclinic pyroxenes (augite, hypersthene) and amphibole, was reported by Monod (1977). The volcanic rocks are spilitized pillow-lavas with a microlitic–porphyric texture. The interstices of the pillow lavas are filled by red micritic limestone of Upper Triassic age and radiolarites (Monod, 1977). According to geological and geochemical evidence, the Beysehir ophiolite formed in a supra-subduction zone tectonic setting (Elitok, 2001; Andrew and Robertson, 2002).

3. Mineralogy and petrography

The metamorphic rocks are strongly foliated amphibolites, interpreted as representing fragments of a dismembered metamorphic sole. A foliation is defined by the subparallel alignment of amphibole-epidote and amphibole-plagioclase crystalloblasts. The amphibolites are generally dark green, the grain size of the amphiboles ranging from 0.8 to 3 mm. The textures are granoblastic, grano-nematoblastic (Fig. 4a and b),

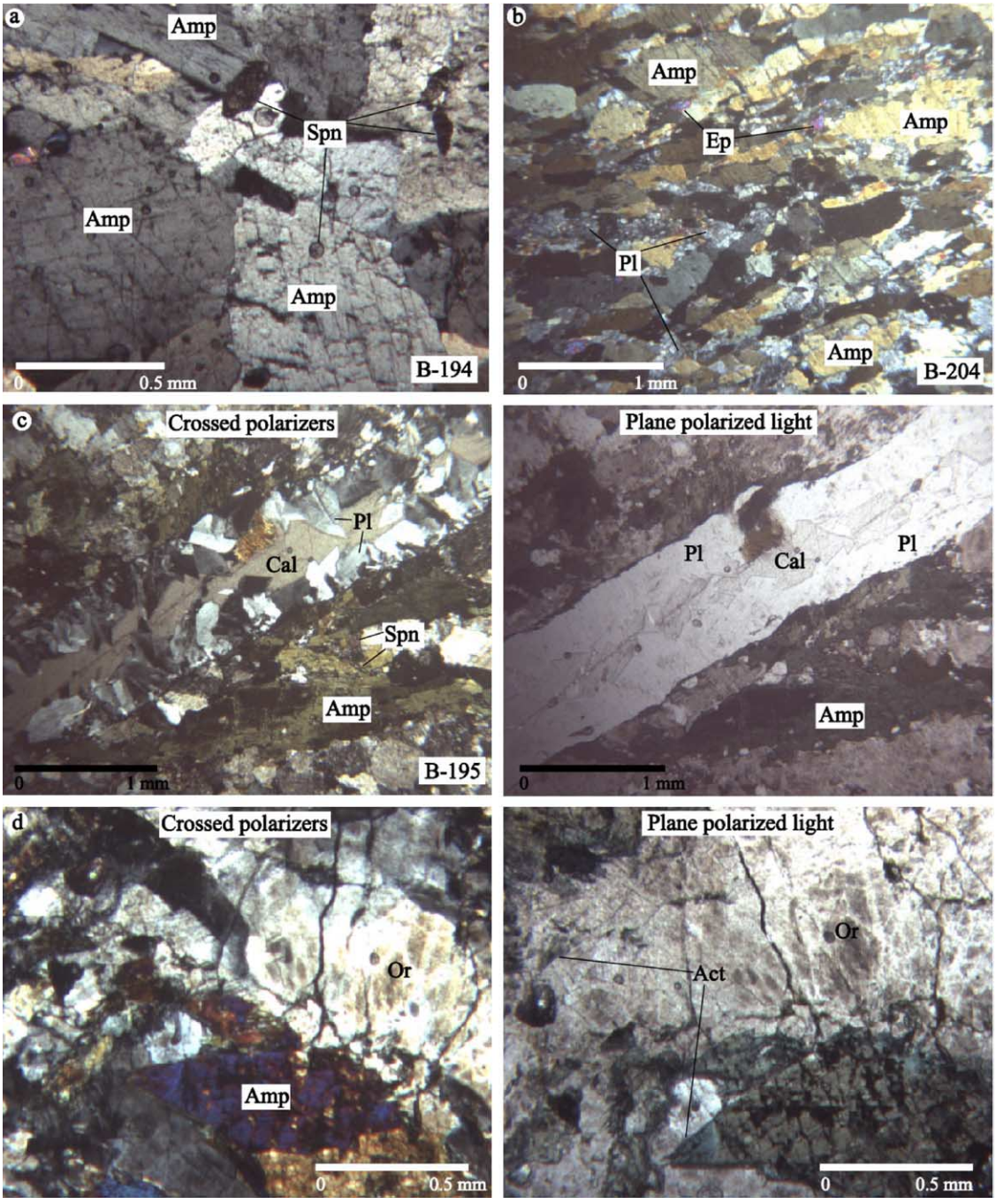

Fig. 4. (a) Photomicrograph of amphibolite exhibiting granoblastic texture; (b) Photomicrograph of amphibolite sample showing grano-nematoblastic texture. Plagioclase in the association is strongly altered to albite and rarely epidote; (c) Photomicrograph of fluid channel in which new plagioclase and calcite develop; (d) Actinolite development in the vein. Mineral abbreviations: amphibole (Amp), plagioclase (Pl), orthoclase (Or), epidote (Ep), calcite (Cal), and sphene (Spn).

porphyroblastic and/or poikiloblastic. The commonest mineral assemblage is amphibole, plagioclase, minerals of the epidote group, sphene and opaque minerals. Additionally, pyroxene, garnet, biotite, calcite, chlorite, apatite occur in some samples. The most frequent mineral assemblages in the amphibolites are given in Table 1. In modal composition, one amphibolite (sample B-188) from the amphibolite facies is composed of hornblende 90%, oligoclase 3%, biotite + chlorite 2%, apatite 1%, sphene + opaque mineral 4%. However, modal contents of the amphibolites are highly variable; hornblende (98–60%), pyroxene (15–20%), garnet (5%), plagioclase (5–35%), epidote (1–15%), biotite + chlorite (1–2%), sphene + apatite + opaque mineral (1–10%).

Table 1
Mineral assemblage in amphibolites of the Beysehir ophiolitic mélange

Sample	Rock name	Texture	Grain size (mm)	Amp	Px	Grt	Pl	Ep	Bt	Cal	Chl	Spn	Ap	Opq
B-186	Amphibolite	Granoblastic	1.2	X			X		X			X		
B-187	Pyroxene-amphibolite	Granoblastic	2.4	X	X		X	X		*X	*X	X	X	
B-188	Amphibolite	Granoblastic	2.2	X			X		X		*X	X		X
B-189	Amphibolite	Granonematoblastic	1	X			X	*X	*X			X		
B-190	Amphibolite	Granoblastic	0.8	X				*X			*X			X
B-191	Amphibolite	Granoblastic	2.6	X				*X	*X	X				X
B-192	Amphibolite	Granoblastic	3	X			X	*X		X				X
B-193	Pyroxene-amphibolite	Nematoblastic	2	X	X		X	X		*X	*X	X	X	
B-194	Amphibolite	Granoblastic	1.4	X			X					X		
B-195	Amphibolite	Granonematoblastic	2.2	X			X	X	X	*X		X	X	
B-196	Amphibolite	Granoblastic	3	X			X	*X			*X	X		
B-197	Amphibolite	Granoblastic	3	X			X	*X				X		
B-198	Amphibolite	Granonematoblastic	1.2	X			X					X		
B-199	Garnet-amphibolite	Granoblastic	1.4	X		X	X	*X				X	X	
B-200	Amphibolite	Granoblastic	1	X			X	*X			*X	X	X	X
B-201	Amphibolite	Granoblastic	1.4	X			X	*X				X		
B-202	Amphibolite	Granoblastic	2	X			X					X		
B-203	Amphibolite	Granoblastic	3	X			X					X		
B-204	Pyroxene-amphibolite	Nematoblastic	1.2	X	X		X	X				X		

(*) Indicating secondary mineral development (mostly in veins).

Primary calcite was not observed, however, calcite is very common in veins as secondary mineralization product. Thus, the amphibolites of the Beysehir metamorphic rocks could have been formed mainly from non-spilitized basalts. Epidote distinguishes the epidote-amphibolite from the amphibolite facies; the only difference is the presence or absence of epidote in rocks of typical basaltic composition. However, epidote and also chlorite could be stable, even within the amphibolite facies, but the bulk composition in which these minerals may appear is restricted (Spear, 1993).

Foliation in the epidote-bearing amphibolite is defined by hornblende and epidote, with plagioclase. Grain boundaries are not always clear, due to the absence of twinning in plagioclase. However, straight grain boundaries between hornblende and plagioclase indicate textural equilibrium. Sample B-195, consisting of amphibole, plagioclase, epidote, biotite, sphene and apatite, shows late mineralization in fluid channels and/or veins 1–3 mm thick. Late minerals developed in the channels are fresh plagioclase and calcite. Euhedral plagioclase can be observed on both sides of the fluid channels (Fig. 4c). This observation shows that mineralization continued after the main metamorphic phase. This late mineralization could be related either to doleritic gabbroic dike injections cross-cutting the Beysehir ophiolite, or to hydrothermal alteration processes.

Petrographic and geochemical results were obtained from amphibolitic blocks which are located to the west of Gencek, and several small amphibolite blocks located to the south of Durak. In these areas amphibolites exhibit a similar geochemical signature.

Amphibolites in the ophiolitic mélange of the Beysehir ophiolite show variable mineral parageneses and textures. For this reason, they were grouped into four groups according to their mineralogical assemblage:

1. Amphibole + garnet + plagioclase ± epidote (as secondary mineral) ± ilmenite ± accessory minerals such as sphene and apatite.
2. Amphiboles + pyroxene + plagioclase ± epidote ± accessory minerals such as sphene, apatite ± chlorite, calcite (as secondary mineral).
3. Amphibole ± plagioclase ± accessory minerals.
4. Amphibole + plagioclase ± epidote ± biotite and muscovite ± accessory minerals.

Pyroxene occurs as equidimensional crystalloblasts, but those of Köycegiz (Fig. 1) are porphyroblasts (Çelik and Delaloye, 2003). In thin section, amphiboles are generally euhedral, ranging from 0.8 to 3 mm in size. Sphene is the most abundant accessory mineral, indicating high temperature conditions. Sphene is located along foliation planes and is locally present within the lineation defined by amphibole crystalloblasts. Sphene is a common mineral in the amphibolites of the Beysehir metamorphic rocks, as in the other metamorphic soles of the Tauride ophiolites such as Lycian (Köycegiz-Yesilova), Mersin and Pozantı-Karsantı. However, sphene is not observed in some of the Beysehir samples. Raase et al. (1986) have proposed that as temperature rises, amphibole will be enriched in Ti, in the presence of a Ti saturating phase. Thus, sphene could be a temperature indicator. The sphene content diminishes towards

the base of the metamorphic sole as observed for example near Köycegiz (Çelik and Delaloye, 2003). This provides additional evidence for the inverted metamorphic zonation of the metamorphic soles. Metamorphic soles at the base of peridotites start with amphibolite facies rocks, passing downwards into epidote-amphibolite and greenschist facies rocks.

4. Geochemistry

4.1. Whole-rock chemistry

Major and trace element analyses (Table 2) were carried out using XRF at Lausanne University. Compositions were determined on glass beads fused in a gold–platinum crucible

Table 2
Major, trace and RE element analyses of amphibolites in the Beysehir ophiolitic mélange

Sample no.	B 186	B 187	B 188	B 189	B 190	B 191	B 192	B 194	B 195	B 196	B 197	B 198	B 201	B 202	B 204
Major elements (wt%)															
SiO_2	44.62	43.02	44.03	44.60	45.30	44.15	44.55	46.61	48.85	44.05	47.07	50.02	47.52	50.12	46.08
TiO_2	2.82	3.07	2.57	2.98	1.96	2.39	2.34	2.01	2.90	2.63	2.04	2.42	1.18	0.54	2.51
Al_2O_3	11.93	15.27	10.31	11.39	8.50	10.74	10.96	8.73	15.97	10.37	9.13	11.61	10.42	7.37	11.71
Fe_2O_3	13.59	11.10	13.55	14.08	12.59	13.29	12.52	12.31	10.75	13.72	12.48	11.84	11.96	12.05	11.81
FeO	0.00	0.00	0.00	0.00	0.00	0.00	0.00	0.00	0.00	0.00	0.00	0.00	0.00	0.00	0.00
MnO	0.18	0.18	0.18	0.18	0.17	0.19	0.17	0.19	0.19	0.18	0.15	0.20	0.27	0.36	0.16
MgO	9.80	4.95	14.70	10.68	16.58	14.07	12.07	14.01	3.99	14.75	13.86	8.76	13.00	15.14	9.57
CaO	11.30	14.87	10.39	11.71	11.57	10.84	13.12	12.51	8.09	10.24	11.73	9.86	11.39	11.03	13.65
Na_2O	2.94	2.39	1.93	2.40	1.19	2.11	1.92	1.50	4.70	1.96	1.83	3.61	1.66	1.36	1.73
K_2O	0.98	1.86	0.35	0.73	0.18	0.47	0.76	0.68	2.32	0.28	0.54	0.56	1.01	0.55	1.36
P_2O_5	0.50	0.74	0.57	0.41	0.20	0.31	0.32	0.32	1.17	0.39	0.17	0.41	0.28	0.01	0.50
LOI	0.98	2.03	1.40	0.88	1.75	1.27	1.54	1.18	1.21	1.38	1.30	0.89	1.36	1.37	1.01
CO_2	0.00	0.00	0.00	0.00	0.00	0.00	0.00	0.00	0.00	0.00	0.00	0.00	0.00	0.00	0.00
Cr_2O_3	0.06	0.02	0.12	0.10	0.17	0.11	0.11	0.12	0.00	0.11	0.14	0.05	0.09	0.13	0.06
NiO	0.02	0.01	0.08	0.05	0.09	0.07	0.05	0.07	0.00	0.07	0.09	0.03	0.05	0.08	0.04
Total	99.71	99.51	100.18	100.18	100.23	100.01	100.41	100.24	100.15	100.13	100.52	100.26	100.17	100.12	100.20
Trace elements (ppm)															
Nb	49	89	31	39	19	33	38	25	106	32	24	36	23	8	39
Zr	189	424	150	199	104	152	162	126	356	157	123	183	119	56	216
Y	25	33	23	25	19	24	22	20	39	25	19	24	29	20	25
Sr	453	710	283	302	184	250	423	224	1185	272	235	170	37	42	227
Rb	9	30	6	8	3	10	10	9	36	7	7	7	9	6	18
Th	5	7	<2<	5	2	<2<	3	<2<	3	3	<2<	6	3	<2<	4
Pb	6	3	8	7	14	10	7	12	<2<	10	11	11	15	18	9
Ga	18	22	16	17	14	16	16	13	18	17	13	15	11	7	18
Zn	120	137	110	117	96	108	102	106	124	111	106	122	117	142	112
Cu	92	19	49	51	56	51	35	20	12	33	<2<	45	150	3	35
Ni	192	59	547	354	622	495	381	483	<2<	504	644	235	341	531	285
Co	70	43	83	81	85	87	76	82	29	84	91	70	82	84	71
Cr	453	152	885	670	1209	766	752	794	3	780	846	368	563	814	403
V	329	250	265	291	192	259	263	197	65	263	190	222	213	139	213
Ba	350	629	106	175	9	122	307	149	930	56	106	62	90	53	326
Sc	39	20	50	47	57	50	42	41	14	53	40	32	52	64	29
As	5	5	6	3	4	4	<3<	3	3	4	<3<	5	4	5	5
Rare earth elements (ppm)															
La		88.00			16.30				97.10				10.80		38.30
Ce		166.00			37.10				203.00				30.50		77.90
Pr		17.80			4.39				22.30				3.90		8.75
Nd		70.00			19.70				94.60				19.40		37.00
Sm		12.20			4.38				17.80				4.88		7.61
Eu		3.99			1.66				6.08				1.61		2.58
Gd		11.50			5.12				16.00				5.61		7.36
Tb		1.58			0.76				2.12				0.98		1.09
Dy		8.20			4.06				10.90				5.82		5.86
Ho		1.53			0.74				1.84				1.17		1.04
Er		3.96			1.88				4.25				3.24		2.62
Tm		0.51			0.23				0.49				0.45		0.33
Yb		2.97			1.32				2.66				2.89		1.85
Lu		0.41			0.18				0.34				0.42		0.25

at 1150 °C from ignited powders to which $Li_2B_4O_7$ was added in the proportion of 1 part of rock to 5 part of flux. REE were analysed by inductively coupled plasma-mass spectrometry (ICP-MS) technique (Actlabs, Ancaster, Ont.).

All of the amphibolite samples have low LOI (<2.03%) suggesting that alteration minerals and hydrated phases were not important. However, as previously mentioned, secondary minerals, such as calcite, chlorite and epidote were identified in veinlets.

On the total alkali versus silica diagram of Rickwood (1989) the amphibolite samples show an alkaline character. The alkaline character of the amphibolites is common among Tauride Belt Ophiolites (Lytwyn and Casey, 1995; Parlak et al., 1995; Polat et al., 1996; Çelik, 2002).

The amphibolites exhibit REE patterns with LREE enrichment (Fig. 5), typical of within-plate basalts (WPB), very similar to those of ocean island basalts in the Azores (White et al., 1979) or to alkali basalts in the Ankara mélange (Floyd, 1993). The primitive mantle-normalized and Mid-Ocean Ridge Basalt (MORB)-normalized spider diagrams also support their WPB or seamount signature. As shown on Fig. 6, they are similar to average Ocean Island Basalt (OIB) patterns and are enriched in incompatible elements such as Rb, Ba, Th and K.

On the Ti–Zr–Y diagram of Pearce and Cann (1973), amphibolites of the Beysehir area plot in the WPB field (Fig. 7a). In the TiO_2–Mn0–P_2O_5 diagram the amphibolites plots in the ocean island basalt field (Fig. 7b). Ti vs V and Zr/Y vs Zr diagrams also indicate the WPB signature (Fig. 7c and d), except for two samples which plot in the Ocean Floor Basalt (OFB) or MORB fields. These two different geochemical affinities (MORB-OIB-like amphibolites and IAT-like amphibolites) were also reported occurring together, in the metamorphic sole of the Lycian ophiolites (Çelik and Delaloye, 2003). Andrew and Robertson (2002) obtained geochemical results from basaltic rocks in the Beysehir ophiolitic mélange showing that they were generated in MORB-supra-subduction zone (SSZ) and seamount settings (within-plate affinities). These rocks could represent protoliths of the amphibolite.

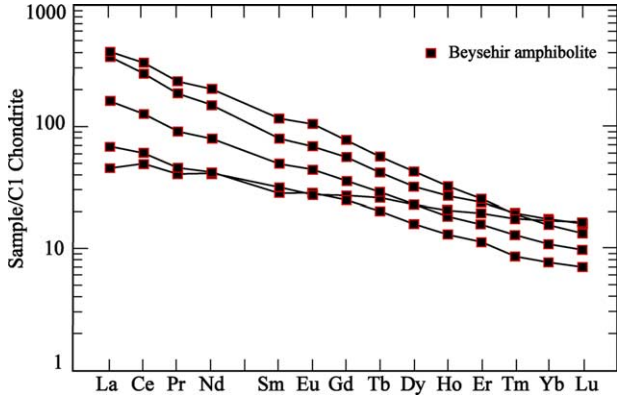

Fig. 5. Chondrite-normalized REE plots for amphibolites in the Beysehir ophiolitic mélange (normalizing values from Sun and McDonough, 1989).

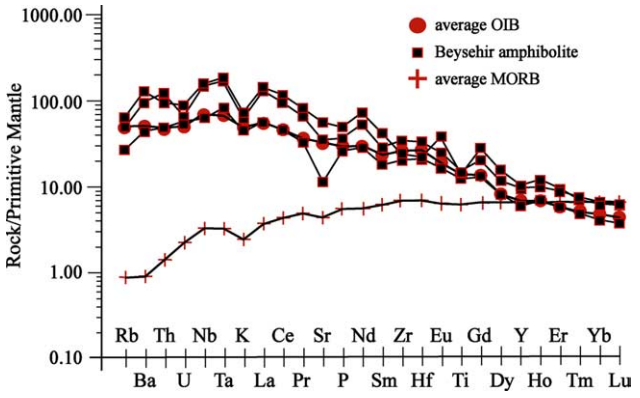

Fig. 6. Primitive mantle-normalized trace element diagram for amphibolites of the Beysehir ophiolitic mélange, and average MORB and OIB (values for MORB and OIB from Sun and McDonough, 1989).

4.2. Mineral chemistry

Mineral analyses were performed on a Cameca SX50 electron microprobe equipped with wavelength dispersive spectrometry at the University of Lausanne. Operating conditions were 15 kV accelerating voltage and 15 nA sample current. Counting times of 10–30 s were applied. Representative mineral analyses are given in Table 3.

4.2.1. Amphibole

According to the nomenclature of Leake et al. (1997), all of the amphiboles are calcic, and cluster in the range from magnesio-hastingsite, pargasite to actinolite. In the first group of parageneses (garnet-amphibolite, sample B-199) the amphiboles, are dominated by magnesio-hornblende and actinolite. Amphiboles of the second (pyroxene-amphibolite, sample B-204) group are characterized by edenite. In the third and fourth group, amphiboles (samples B-194, B-196, B-197, B-198 and B-202) are dominated by magnesio-hornblende, actinolite, magnesio-hastingsite and edenite, except for sample B-195 from the fourth group which is characterized by pargasite and ferropargasite (Fig. 8). Amphibole compositions are characterized by SiO_2=(38.02–54.3%), Al_2O_3=(1.5–12.8%), FeO=(10.03–14.67%), K_2O=(0.2–1.8%), MgO=(5.5–15.7%), Mg*=(0.3–0.8). As mentioned before, the amphibolites were grouped according to their mineralogical assemblages. However, there is no systematic variation in their calcic amphibole composition. Compositional changes in amphiboles suggest facies changes with decreasing or increasing temperature during amphibole crystallisation. However, the abrupt change from actinolitic to Al-rich hornblendic compositions is attributed to a miscibility gap between actinolite and Al-rich hornblende (Smelik et al., 1990; Bégin and Carmichael, 1992). A change in composition from Al-rich hornblende in the core to actinolite in the rim of crystalloblasts (samples B-196 and B-202) may indicate a change in the physico-chemical conditions. The TiO_2

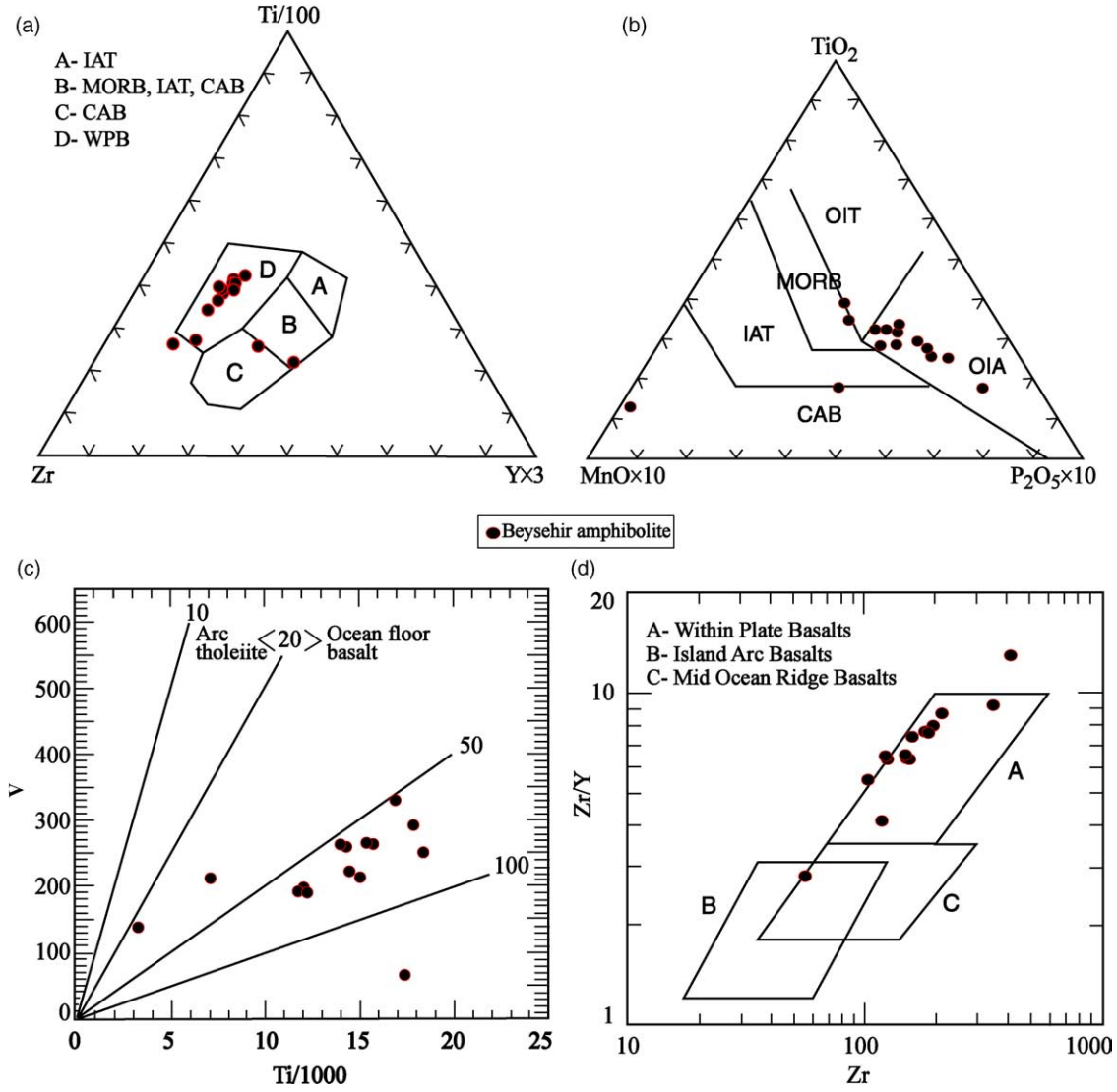

Fig. 7. (a) Ti–Zr–Y tectonomagmatic discrimination diagram of amphibolites in the Beysehir ophiolitic mélange (after Pearce and Cann, 1973); (b) TiO_2–MnO–P_2O_5 discrimination diagram (after Mullen, 1983); (c) Plot of Ti versus V (after Shervais, 1982); (d) Zr/Y versus Zr discrimination diagram (after Pearce and Norry, 1979).

content of amphiboles varies between amphibole types. Actinolites in samples B-196 and B-202 show TiO_2 contents below 0.14 wt%. Whereas, those of magnesio-hastingsite, edenite and magnesio-hornblende, according to the nomenclature of Leake et al. (1997), have between 0.34 and 1.59 wt% TiO_2. Biotite and chlorite were very seldom observed as alteration products of the amphiboles.

4.2.2. Feldspar

Feldspars have different chemical compositions (Fig. 9). In thin sections from samples B-196 and B-197 feldspars are rarely observed in contact with amphibole, since they occur mainly in veins. Feldspars in contact with amphiboles are altered and have an albitic composition (Ab_{98}–Or_1). On the contrary, feldspars in veins have compositions in the range from albite to orthoclase and anorthoclase (Ab_{30}-Or_{69}). Actinolite and epidote replace hornblende on both sides of the veins. Actinolite was observed as fibrous crystals among the feldspars (Fig. 4d). The formation of potassic feldspar in high-grade metamorphic rocks is due to instability of micas in P–T environment, but the protolith of these rocks, ‘alkali basalt’ does not contain any mica which could produce potassium-rich feldspar.

Since the alkali feldspars are observed in veins, and not in contact with amphiboles, we consider that hydrothermal alteration was active and efficient in the oceanic environment. Potassic alteration is a relatively high temperature type of alteration, which results from potassium enrichment. This style of alteration can form before the complete crystallization of a magma, as evidenced by the sinuous, and discontinuous vein patterns. Potassic alteration can also occur in deeper plutonic environments, where orthoclase

Table 3
Representative microprobe analyses of amphiboles, pyroxenes, garnets and feldspars in amphibolites from the Beysehir ophiolitic mélange

Sample	Amphiboles																
	B-194-2c	B-194-2r	B-195-5c	B-195-6c	B-196-1c	B-196-2c	B-196-2r	B-197-2c	B-197-2r	B-198-1c	B-199-1c	B-199-1r	B-199-2c	B-199-2r	B202-4c	B204-6c	B204-6r
SiO_2	46.160	46.200	38.020	40.930	46.940	50.130	46.980	47.990	46.640	45.140	46.860	47.270	47.080	46.520	48.550	45.800	46.780
TiO_2	1.400	1.380	11.020	1.220	1.390	0.940	1.500	1.220	1.620	0.920	0.720	0.740	0.590	0.570	0.810	0.740	0.680
Al_2O_3	9.950	10.310	9.230	11.760	9.130	6.400	9.420	8.840	9.800	9.600	10.240	9.070	10.100	9.880	7.030	10.660	10.330
Fe_2O_3(c)	1.650	0.710	0.000	1.450	3.670	1.070	2.680	2.120	1.540	4.250	6.120	3.060	5.180	5.420	6.410	0.000	0.490
FeO(c)	10.770	12.140	14.360	19.140	8.250	10.910	9.190	9.320	10.470	11.960	7.330	10.510	8.690	8.470	5.740	13.050	12.630
MnO	0.180	0.210	0.240	0.390	0.180	0.160	0.220	0.190	0.180	0.260	0.900	0.900	0.850	0.840	0.430	0.200	0.220
MgO	13.520	12.850	5.590	7.680	14.580	14.820	14.340	14.410	13.670	11.770	12.930	12.310	12.740	12.730	15.160	12.380	12.530
CaO	11.930	12.000	17.090	11.510	11.660	12.050	11.800	11.760	11.660	11.560	11.050	11.250	11.410	11.420	11.180	12.450	12.320
Na_2O	1.980	2.000	1.650	2.480	2.000	1.580	2.100	1.810	2.230	1.910	1.570	1.620	1.490	1.440	1.390	1.490	1.420
K_2O	0.690	0.630	1.190	1.590	0.430	0.290	0.390	0.380	0.390	0.710	0.490	0.460	0.580	0.550	0.330	1.120	0.810
F	0.000	0.000	0.140	0.190	0.000	0.030	0.060	0.000	0.000	0.050	0.010	0.000	0.000	0.000	0.060	0.000	0.000
H_2O(c)	2.060	2.060	1.890	1.860	2.080	2.070	2.060	2.080	2.070	2.010	2.080	2.050	2.080	2.060	2.050	2.040	2.050
Sum Ox%	100.290	100.500	100.370	100.130	100.320	100.420	100.700	100.120	100.280	100.110	100.310	99.230	100.790	99.910	99.120	99.950	100.270
Si	6.705	6.717	5.825	6.290	6.759	7.199	6.751	6.904	6.748	6.661	6.751	6.926	6.778	6.762	7.010	6.727	6.814
Ti	0.153	0.151	1.269	0.141	0.150	0.102	0.163	0.132	0.176	0.102	0.078	0.082	0.063	0.062	0.088	0.081	0.074
Al/Al ^{IV}	1.295	1.283	1.665	1.710	1.241	0.801	1.249	1.096	1.252	1.339	1.249	1.074	1.222	1.238	0.990	1.273	1.186
Al ^{VI}	0.408	0.484	0.000	0.420	0.308	0.283	0.347	0.403	0.420	0.330	0.489	0.493	0.491	0.455	0.206	0.572	0.587
Fe^{3+}	0.180	0.077	0.000	0.167	0.397	0.115	0.289	0.230	0.168	0.472	0.663	0.337	0.562	0.593	0.696	0.000	0.054
Fe^{2+}	1.308	1.477	1.840	2.460	0.993	1.310	1.104	1.122	1.267	1.475	0.884	1.288	1.047	1.030	0.694	1.603	1.539
Mn^{2+}	0.022	0.026	0.031	0.051	0.022	0.019	0.027	0.023	0.023	0.033	0.110	0.111	0.103	0.103	0.053	0.025	0.027
Mg	2.928	2.786	1.276	1.760	3.130	3.171	3.071	3.090	2.947	2.588	2.776	2.688	2.734	2.757	3.263	2.710	2.720
Ca	1.857	1.869	2.805	1.895	1.799	1.854	1.816	1.813	1.808	1.827	1.706	1.766	1.761	1.779	1.730	1.960	1.923
Na	0.556	0.565	0.489	0.739	0.559	0.439	0.585	0.504	0.624	0.545	0.440	0.461	0.415	0.407	0.390	0.425	0.402
K	0.128	0.118	0.233	0.311	0.079	0.053	0.071	0.070	0.073	0.134	0.091	0.086	0.106	0.102	0.061	0.210	0.150
F	0.000	0.000	0.068	0.092	0.000	0.015	0.027	0.000	0.000	0.022	0.003	0.000	0.002	0.000	0.026	0.000	0.000
Cl	0.000	0.000	0.000	0.002	0.003	0.000	0.000	0.000	0.000	0.002	0.003	0.000	0.000	0.001	0.000	0.000	0.005
OH	2.000	2.000	1.932	1.907	1.997	1.985	1.972	2.000	2.000	1.976	1.994	2.000	1.998	1.999	1.974	2.000	1.995
Sum Cat#	17.542	17.552	17.435	17.945	17.437	17.346	17.472	17.387	17.505	17.506	17.236	17.314	17.282	17.288	17.181	17.587	17.475
XMg	0.691	0.654	0.410	0.417	0.759	0.708	0.736	0.734	0.699	0.637	0.759	0.676	0.723	0.728	0.825	0.628	0.639

Sample	Pyroxenes					Sample	Garnets			
	B-187-5	B-187-7	B-204-1	B-204-2	B-204-3		B-199-1	B-199-2	B-199-3	B-199-4
SiO_2	51.870	48.670	52.900	52.590	53.000	SiO_2	37.740	37.050	37.110	36.860
TiO_2	0.110	0.470	0.080	0.110	0.110	TiO_2	0.040	0.060	0.100	0.140
Al_2O_3	2.790	5.700	2.000	2.630	2.070	Al_2O_3	20.220	19.990	19.970	20.050
Cr_2O_3	0.010	0.000	0.020	0.000	0.010	Cr_2O_3	0.060	0.150	0.000	0.000
Fe_2O_3(c)	11.380	4.870	1.510	0.880	0.240	Fe_2O_3(c)	1.450	2.890	2.920	3.000
FeO(c)	4.470	6.890	6.120	6.950	7.350	FeO	18.440	16.580	16.520	16.400
MnO	0.460	0.290	0.180	0.210	0.230	MnO	8.690	10.220	10.630	11.080
MgO	8.280	9.700	12.860	12.530	12.710	MgO	5.070	4.840	4.760	4.810
CaO	16.960	22.220	22.490	22.320	22.750	CaO	6.920	6.870	6.780	6.250
Na_2O	4.460	1.230	1.140	1.050	0.880	Sum Ox%	98.640	98.640	98.790	98.590
Sum Ox%	100.790	100.040	99.300	99.270	99.370					
						Si	3.004	2.963	2.966	2.954
Si	1.937	1.836	1.974	1.965	1.980	Ti	0.002	0.003	0.006	0.009

Ti	0.003	0.013	0.002	0.003	0.003	Al/Al^{IV}	0.000	0.037	0.034	0.046
Al/Al^{IV}	0.063	0.164	0.026	0.035	0.020	Al^{VI}	1.897	1.847	1.847	1.848
Al^{VI}	0.060	0.089	0.061	0.081	0.071	Cr	0.004	0.010	0.000	0.000
Cr	0.000	0.000	0.000	0.000	0.000	Fe^{3+}	0.087	0.174	0.175	0.181
Fe^{3+}	0.320	0.138	0.042	0.025	0.007	Fe^{2+}	1.228	1.109	1.104	1.099
Fe^{2+}	0.140	0.217	0.191	0.217	0.230	Mn^{2+}	0.586	0.693	0.720	0.752
Mn^{2+}	0.015	0.009	0.006	0.007	0.007	Mg	0.602	0.577	0.567	0.574
Mg	0.461	0.545	0.715	0.698	0.708	Ca	0.590	0.589	0.581	0.537
Ca	0.678	0.898	0.899	0.894	0.910	Sum Cat#	8.000	8.000	8.000	8.000
Na	0.323	0.090	0.082	0.076	0.064	Pyrope	20.025	19.444	19.081	19.389
Sum Cat#	4.000	4.000	4.000	4.000	4.000	Almandine	40.842	37.370	37.160	37.100
Wo(Ca)	53.032	54.083	49.800	49.405	49.275	Spessartine	19.500	23.348	24.222	25.386
En(Mg)	36.044	32.831	39.622	38.583	38.294	Andradite	4.375	8.540	8.650	8.871
Fs(Fe^{2+})	10.924	13.085	10.578	12.012	12.431	Uvarovite	0.197	0.471	0.001	0.001
XMg	0.767	0.715	0.789	0.763	0.755	Grossulaire	15.061	10.827	10.885	9.254
						XMg	0.329	0.342	0.339	0.343

Sample	Plagioclases										
	B-195-17	B-195-18	B-197-5	B-197-1	B-202-8	B-202-9	B-202-10	B-204-4	B-204-8	B-204-10	B-204-11
SiO_2	64.470	64.900	68.080	66.870	68.870	68.650	68.730	66.120	59.390	63.000	59.030
Al_2O_3	22.580	22.410	19.500	19.840	19.280	19.600	19.640	21.160	25.400	22.640	26.050
Fe_2O_3	0.060	0.060	0.070	0.000	0.030	0.070	0.100	0.080	0.090	0.080	0.120
MgO	0.010	0.000	0.000	0.020	0.010	0.000	0.000	0.020	0.000	0.030	0.000
CaO	3.880	3.450	0.430	0.440	0.060	0.180	0.290	1.540	7.620	3.010	8.230
BaO	0.000	0.010	0.010	0.010	0.000	0.000	0.000	0.000	0.020	0.060	0.010
Na_2O	9.660	9.640	11.420	9.580	11.830	11.830	11.510	9.690	7.270	8.660	6.860
K_2O	0.200	0.190	0.120	0.260	0.040	0.050	0.060	0.560	0.280	0.680	0.220
Sum Ox%	100.870	100.660	99.630	97.020	100.130	100.380	100.330	99.190	100.070	98.170	100.520
Si	2.825	2.842	2.987	2.992	3.003	2.989	2.991	2.920	2.651	2.828	2.626
Al/Al^{IV}	1.166	1.157	1.008	1.046	0.991	1.006	1.008	1.101	1.336	1.197	1.365
Al^{VI}	0.000	0.000	0.002	0.000	0.001	0.002	0.003	0.003	0.003	0.003	0.004
Fe^{3+}	0.002	0.002	0.000	0.001	0.001	0.000	0.000	0.001	0.000	0.002	0.000
Mg	0.001	0.000	0.020	0.021	0.003	0.009	0.014	0.073	0.365	0.145	0.392
Ca	0.182	0.162	0.000	0.000	0.000	0.000	0.000	0.000	0.000	0.001	0.000
Na	0.821	0.818	0.972	0.831	1.000	0.999	0.971	0.830	0.630	0.754	0.591
K	0.011	0.011	0.007	0.015	0.002	0.003	0.003	0.032	0.016	0.039	0.013
Sum Cat#	5.007	4.993	4.997	4.907	5.002	5.007	4.990	4.959	5.001	4.969	4.992
Ab	80.957	82.557	97.269	95.826	99.481	98.904	98.310	88.779	62.306	80.304	59.342
An	17.956	16.352	2.043	2.422	0.287	0.847	1.374	7.814	36.098	15.421	39.378
Or	1.087	1.081	0.678	1.726	0.232	0.248	0.316	3.398	1.559	4.172	1.268

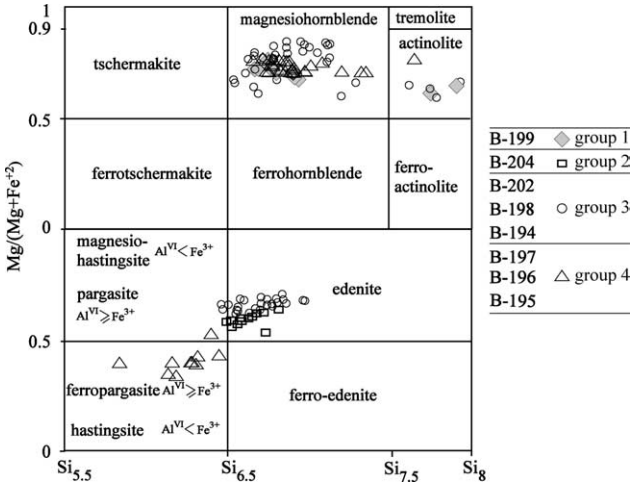

Fig. 8. Chemical composition of amphiboles in amphibolite in the Beysehir ophiolitic mélange. (after Leake et al., 1997).

will be formed. Another possibility is that alkali feldspar, and relatively low temperature minerals such as actinolite and epidote in the veins, developed during dike injection in the oceanic environment.

Sample B-204 shows a nematoblastic texture and consists of amphibole, pyroxene, plagioclase, epidote and sphene. Plagioclase compositions are in the range albite to andesine. Plagioclase was also affected by hydrothermal alteration and developed an albite to anorthoclase composition.

4.2.3. Clinopyroxene

Clinopyroxene occurs as xenomorphic equidimensional crystalloblasts. In sample B-187 clinopyroxene is Ca-rich. In sample B-204 clinopyroxene is diopside (Fig. 10), the common metamorphic mineral of high-grade metamorphic terrains.

4.2.4. Garnet

Garnet was not an abundant mineral in the amphibolites. Only one garnet from sample B-199 was analysed by

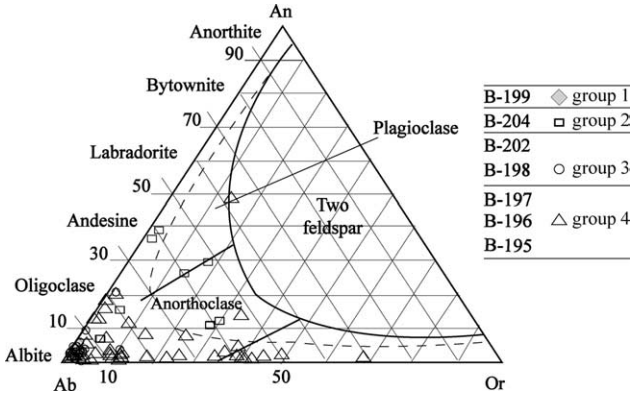

Fig. 9. Feldspar ternary diagram showing plagioclase compositions in amphibolites in the Beysehir ophiolitic mélange.

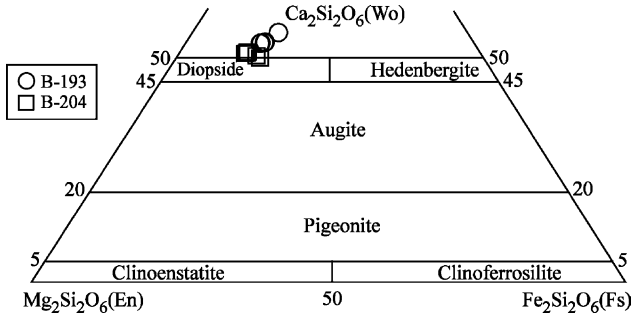

Fig. 10. Chemical composition of pyroxenes in amphibolites from samples B-187 and B-204.

microprobe. It has the composition $Alm_{37–40}$ $Prp_{19–20}$ $Sps_{19–25}$ $Grs_{9–15}$.

5. Geothermobarometry

The amphibolites do not contain suitable mineral parageneses for the calculation of the P–T conditions of metamorphism. For this reason geothermometric studies were carried out using only amphibole-plagioclase couples (e.g. Holland and Blundy, 1994).

Owing to the complex composition of amphiboles, the presence of several miscibility gaps between end-members, and uncertainties at the estimation of $Fe^{+3}/\sum Fe$ from microprobe data, amphibole-plagioclase thermometers are not considered to be entirely reliable.

Sample B-204 was selected for the estimation of the physical conditions at time of metamorphism, because amphiboles and plagioclases show clear contacts at their boundaries and the amphiboles are only of edenite composition. The calibrations of Holland and Blundy (1994) were used and, because quartz is absent in the assemblage, the edenite-richterite thermometer was used in

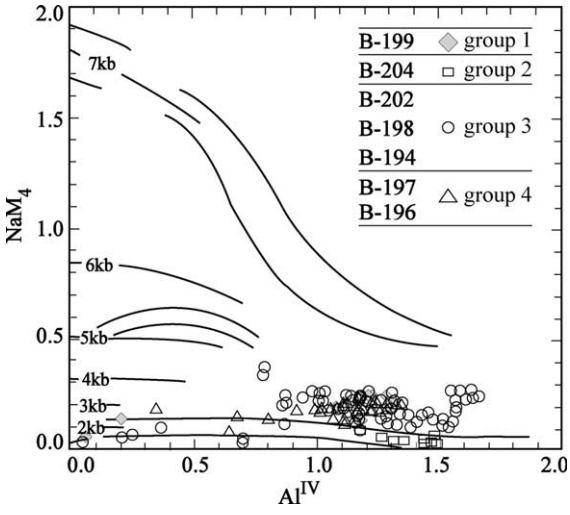

Fig. 11. Comparison of Na^{M4} and Al^{IV} for amphibole from amphibolites of the Beysehir ophiolitic mélange (after Brown, 1977).

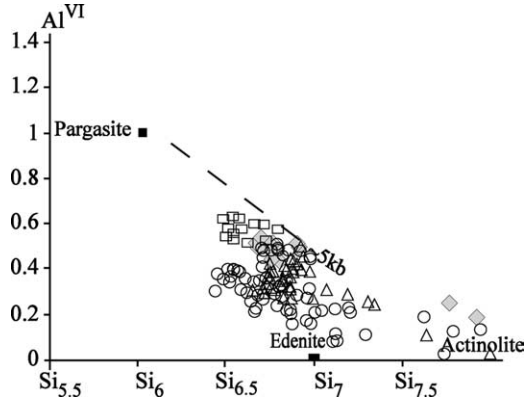

Fig. 12. Al^{VI} versus Si diagram after Raase (1974) for amphiboles in the amphibolites.

the formula. The thermometer applied to several amphibole and plagioclase couples in contact with each other, yielded temperatures between 582 and 603 ± 40 °C.

The geobarometric study was performed on amphibole crystalloblasts using electron microprobe data. Pressure estimates were calculated according to the proportions of Na^{M4}–Al^{IV} and Al^{VI}–Si numbers. As shown in the Na^{M4}–Al^{IV} pressure diagram (Fig. 11) most of the samples are stable, and cluster around 3–4 kb when they are represented by edenite, magnesio-hornblende and magnesio-hastingsite. The Al^{VI}–Si diagram also show that the calcic amphiboles developed at a pressure less than 5 kb (Fig. 12).

As pressure increases, a negative correlation is observed between the Al^{VI} and Al^{IV} content of the amphiboles by increasing of the octahedral Al content, compared with tetrahredal Al content. Fig. 13, show a positive correlation of the Ti and of Al^{IV} content of Ca-amphiboles. As Ti and Al^{IV} contents decrease, actinolite appears in the rock, meaning that the metamorphic temperature was lower. However, Hynes (1982) argues that there is no systematic variation in Na, Na^{M4}, Al total or Al^{VI} as a function of pressure. He suggested that these uncertainties could be due to a variation in oxidation state or analytical differences between laboratories. Another reason is the existence of a compositional gap between actinolite and hornblende in greenschist-amphibolite facies. The effect of bulk rock composition could also have an affect.

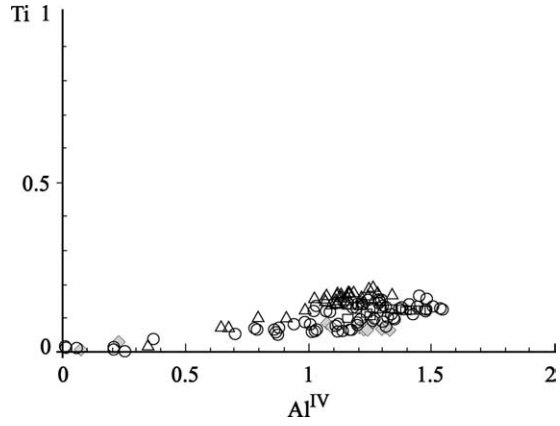

Fig. 13. Ti versus Al^{IV} diagram for amphiboles.

P–T conditions and estimations of the geodynamic environment for the metamorphic sole rocks are similar in all the Tauride Belt ophiolites (Çelik, 2002). It is, therefore, proposed that the amphibolites of the Beysehir ophiolitic mélange were metamorphosed in amphibolite facies at about 550–600 °C and at less than 5 kb pressure.

6. Possible protoliths of the amphibolites

Geochemical criteria can distinguish between *ortho*- and *para*-amphibolites. According to the Cr versus TiO_2 diagram of Leake (1964), *ortho*-amphibolites plot outside the outlined area (Fig. 14a). Cr values are between 152 and 1209 ppm. TiO_2 values are between 0.54 and 3.07 wt%. On the other hand they plot on the fractionation trend typical for igneous rocks on a Zr/TiO_2–Nb/Y diagram, with a composition of alkali basalt and basanite (Fig. 14b).

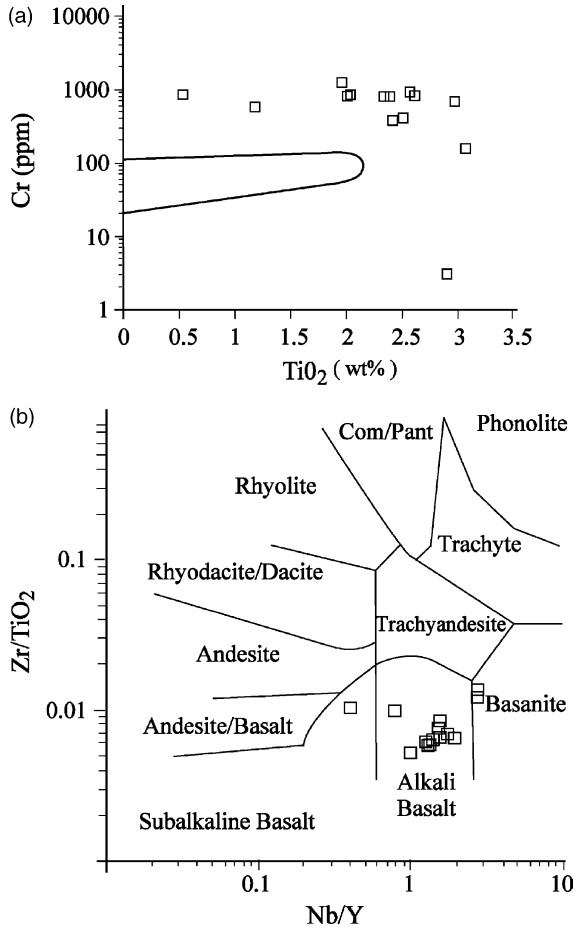

Fig. 14. (a) Cr versus TiO_2 for the amphibolites. The outside of ringed area represents igneous protoliths (after Leake, 1964); (b) Nb/Y vs Zr/TiO_2 diagram showing possible protoliths for amphibolites of the Beysehir ophiolitic mélange (after Winchester and Floyd, 1977).

Similar geological affinities were inferred for the Antalya, the Lycian and the Pozantı-Karsantı amphibolites (Çelik and Delaloye, 2001, 2003).

According to geochemical and petrographic observations on the metamorphic rocks, possible protoliths of the amphibolites are within-plate alkali basalts (seamounts). All along the Tauride Belt Ophiolites the amphibolites are cut by dolerite dikes (e.g. Lycian ophiolites, Çelik and Delaloye, 2003; Mersin ophiolite, Parlak et al., 1995; Pozantı-Karsantı ophiolites, Lytwyn and Casey, 1995; Polat et al., 1996; Çelik, 2002).

The cooling age of the Beysehir amphibolites is estimated as 91.1 ± 1.1 Ma (Çelik et al., under review). Similar ages were obtained from amphibolites of the other Tauride Belt Ophiolites (Thuizat et al., 1981; Dilek et al., 1999; Parlak and Delaloye, 1999; Çelik et al., under review). The amphibolites in the Beysehir ophiolitic mélange and in other metamorphic sole rocks along the Tauride Belt Ophiolites were therefore metamorphosed in the Neotethyan Ocean at the same time.

The matrix of the Beysehir ophiolitic mélange is not metamorphosed, but contains occasional ophiolite-related amphibolites as thrust slices or blocks. The amphibolites were incorporated into the ophiolitic melange after they were metamorphosed as part of a metamorphic sole at the base of peridotites during the northward subduction of a branch of Neotethys. Andrew and Robertson (2002) reported electron microprobe data on chrome spinel grains from peridotite from the Beysehir that support a supra-subduction zone origin. After subduction of oceanic crust in Early Late Cretaceous, a supra-subduction zone type ophiolite was generated in the Neotethyan ocean (Fig. 15a). During this period, an ocean island basalt forming a seamount (protolith of the amphibolite) was accreted and metamorphosed in the subduction zone. The amphibolites were incorporated in the ophiolitic melange from time to time during the Late Cretaceous by tectonic forces. Finally the ophiolite and the subduction/accretionary complex was thrust onto the Tauride Platform (Fig. 15b).

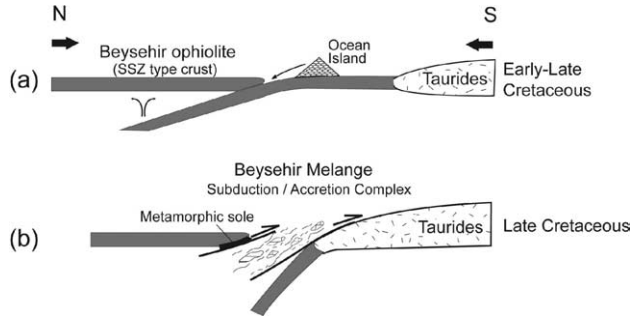

Fig. 15. Tectonic cartoons showing the evolution of the ophiolites and the emplacement of metamorphic sole and dike rocks.

7. Summary and conclusions

Ophiolite-related metamorphic rocks in the Beysehir ophiolitic mélange exhibit four different mineral parageneses and show mainly granoblastic, grano-nematoblastic, porphyroblastic or poikiloblastic textures. The amphiboles have a calcic composition and are represented by edenite, magnesio-hastingsite, magnesio-hornblende and actinolite. Some amphibole crystals show compositional variations from core to rim. These variations indicate retrograde changes of the metamorphic conditions. Plagioclase is albite, oligoclase and andesine. However, in veins the feldspars are albite and potassium-rich feldspar. In one veined sample, plagioclase was observed as neoformation euhedral crystals on both sides of the fluid channel. Calcite was also observed between plagioclase crystals along the vein. The occurrence of calcite indicates that mineralization continued after the main metamorphic phase. This late mineralization phase may be related either to doleritic gabbroic dike injection cutting the Beysehir Ophiolite or to hydrothermal alteration processes.

Primitive mantle-normalized incompatible trace element diagram and REE patterns observed for the amphibolites show a close similarity to the pattern of typical ocean island basalt (OIB) from seamounts. The tectonomagmatic discrimination diagram, based on immobile trace elements, indicates a within plate basalt (WPB) environment.

The origin of the amphibolite rocks is igneous and the protolith of the amphibolites could be basalt and/or gabbro. Absence of plagioclase in some amphibolites suggests a derivation from ultramafic cumulates such as pyroxenite or aphyric basalt.

The petrographic, mineralogical and geochemical characteristics of amphibolites from the Beysehir ophiolitic mélange are very similar to other studied metamorphic sole rocks of the Tauride Belt Ophiolites (e.g. Lycian and Antalya ophiolites, Çelik and Delaloye, 2003; Mersin ophiolite, Parlak et al., 1995).

In conclusion, during the Late Cretaceous (91.1 ± 1.1 Ma) alkali basalts or seamounts were accreted in a subduction zone where they were metamorphosed around 550–600 °C and <5 kb. Later these rocks were tectonically incorporated into an ophiolitic mélange and emplaced on the Tauride carbonate platform to the south.

Acknowledgements

This research was supported by the Swiss National Research Foundation. The authors thank Fabio Capponi for performing major- and trace-element analyses. We thank Ergüzer Bingöl for constructive suggestions. The authors thank Theo Andrew for his assistance in the field. The manuscript greatly benefited from comments by Alastair Robertson, Robin Gill and Anthony Barber.

References

Andrew, T., Robertson, A.H., 2002. The Beysehir-Hoyran-Hadim Nappes: genesis and emplacement of Mesozoic marginal and oceanic units of the northern Neotethys in southern Turkey. Geological Society, London 159, 529–543.

Bégin, N.J., Carmichael, D.M., 1992. Textural and compositional relationship of Ca-amphiboles in metabasites of the Cape Smith Belt, Northern Quebec: implications for a miscibility gap at medium pressure. Journal of Petrology 33, 1317–1343.

Brown, E.H., 1977. The crossite content of Ca-Amphibole as a guide to pressure of metamorphism. Journal of Petrology 18, 53–72.

Çelik, Ö.F., 2002. Geochemical, petrological and geochronological observations on the metamorphic rocks of the Tauride Belt Ophiolites (S.Turkey). PhD Thesis Section des Sciences de la Terre, Université de Genève, Terre and Environnement, 39, 257 p.

Çelik, Ö.F., Delaloye, M., 2001. Geochemical character and tectonic environment of the ophiolite-related metamorphic rocks and their mafic dike swarms in the Pozanti-Karsanti Ophiolite: new age constraints on the metamorphic sole rocks and dike swarms. Fourth International Turkish Geology Symposium (ITGS IV), Adana/Turkey. English Abstract, p. 238.

Çelik, Ö.F., Delaloye, M.F., 2003. Origin of metamorphic soles and their post-kinematic mafic dyke swarms in the Antalya and Lycian ophiolites, SW Turkey. Geological Journal 38, 235–256.

Çelik, Ö.F., Delaloye, M., Feraud, G., in review. Precise $^{40}Ar^{39}Ar$ ages from the metamorphic sole rocks of the Tauride Belt Ophiolites, Southern Turkey: implications for the rapid cooling history.

Collins, A.S., Robertson, A.H.F., 1998. Processes of Late Cretaceous to Late Miocene episodic thrust-sheet translation in the Lycian Taurides, SW Turkey. Journal of the Geological Society, London 155, 759–772.

Dilek, Y., Thy, P., Hacker, B., Grundvig, S., 1999. Structure and Petrology of Tauride ophiolites and mafic dike intrusions (Turkey): implications for the Neotethyan ocean. Geological Society of America Bulletin 111, 1192–1216.

Elitok, Ö., 2001. Geochemistry and tectonic significance of the Sarkikaraagaç Ophiolite in the Beysehir-Hoyran Nappes, SW Turkey. Fourth International Symposium on Eastern Mediterranean Geology, Proceedings, pp. 181–196.

Floyd, P.A., 1993. Geochemical discrimination and petrogenesis of alkalic basalt sequences in part of the Ankara mélange, central Turkey. Journal of the Geological Society, London 150, 541–550.

Gutnic, M., Monod, O., Poisson, A., Dumont, J.F., 1979. Geologie des Taurides Occidentales (Turquie). Memoires de la Societe Geologique de France 137, 1–112.

Holland, T.J.B., Blundy, J.D., 1994. Non-ideal interactions in calcic amphiboles and their bearing on amphibole-plagioclase thermometry. Contributions to Mineralogy and Petrology 116, 433–447.

Hynes, A., 1982. A comparison of amphiboles from medium- and low-pressure metabasites. Contributions to Mineralogy and Petrology 81, 119–125.

Leake, B.E., 1964. The chemical distinction between ortho-and para-amphibolites. Journal of Petrology 5, 238–254.

Leake, B.E., Woolley, A.R., Arps, C.E.S., Birch, W.D., Gilbert, M.C., Grice, J.D., Hawthorne, F.C., Kato, A., Kisch, H.J., Krivovichev, V.G., Linthout, K., Laird, J., Mandarino, J., Maresch, W.V., Nickel, E.H., Rock, N.M.S., Schumacher, J.C., Smith, D.C., Stephenson, N.C.N., Ungaretti, L., Whittaker, E.J.W., Youzhi, G., 1997. Nomenclature of amphiboles: Report of the subcommittee on amphiboles of the International Mineralogical Association, commission on new minerals and mineral names. American Mineralogist 82, 1019–1037.

Lytwyn, J.N., Casey, J.F., 1995. The geochemistry of postkinematic mafic dike swarms and subophiolitic metabasites, Pozantı-Karsantı ophiolite, Turkey: evidence for ridge subduction. Geological Society of America Bulletin 7, 830–850.

Monod, O., 1977. Récherches géologiques dans le Taurus occidental au sud de Beysehir (Turquie). PhD Thesis, Université de Paris Sud, Orsay, 450 p.

Mullen, E.D., 1983. $Mn0/Ti0_2/P_2O_5$: a minor element discriminant for basaltic rocks of oceanic environment and its implication for petrogenesis. Earth and Planetary Science Letters 62, 53–62.

Özgül, N., 1984. Stratigraphy and tectonic evolution of the central Taurus. In: Tekeli, O., Göncüoglu, M.C. (Eds.), Geology of the Taurus Belt Proceedings of the International Tauride Symposium. Mineral Research and Exploration Institute of Turkey (MTA) Publications, , pp. 77–90.

Parlak, O., Delaloye, M., 1999. Precise $^{40}Ar/^{39}Ar$ ages from the metamorphic sole of the Mersin ophiolite (Southern Turkey). Tectonophysics 301, 145–158.

Parlak, O., Delaloye, M., Bingöl, E., 1995. Origin of sub-ophiolitic metamorphic rocks beneath the Mersin ophiolite. Southern Turkey. Ofioliti 20, 97–110.

Pearce, J.A., Cann, J.R., 1973. Tectonic setting of basic volcanic rocks determined using trace element analysis. Earth and Planetary Science Letters 19, 290–300.

Pearce, J.A., Norry, M.J., 1979. Petrogenetic implications of Ti, Zr, Y and Nb variations in volcanic rocks. Contributions to Mineralogy and Petrology 69, 33–47.

Polat, A., Casey, J.F., Kerrich, R., 1996. Geochemical characteristics of accreted material beneath the Pozantý-Karsantý Ophiolite, Turkey: intra-oceanic detachment, assembly and obduction. Tectonophysics 263, 249–276.

Raase, P., 1974. Al and Ti contents of hornblende, indicators of pressure temperature of regional metamorphism. Contributions to Mineralogy and Petrology 45, 231–236.

Raase, P., Raith, M., Ackermand, D., Lal, R.K., 1986. Progressive metamorphism of mafic rocks from greenschist to granulite facies in the Dharwar Craton of South India. Journal of Geology 94, 261–282.

Rickwood, P.C., 1989. Boundary lines within petrologic diagrams which use oxides of major and minor elements. Lithos 22, 247–263.

Ricou, L.E., Argyriadis, I., Marcoux, J., 1975. L'axe calcaire du Taurus, un alignement de fenêtres arobo-africaines sous des nappes radiolaritiques, ophiolitiques et métamorphiques. Bulletin de la Société géologique de France 17, 1024–1043.

Robertson, A.H., 2000. Mesozoic-Tertiary tectonic-sedimentary evolution of a south Tethyan oceanic basin and its margins in southern Turkey. In: Bozkurt, E., Winchester, J.A., Piper, J.D.A. (Eds.), Tectonics and Magmatism in Turkey and Surrounding Area. Geological Society of London Special Publication, , pp. 97–138.

Robertson, A.H.F., 2002. Overview of genesis and emplacement of Mesozoic ophiolites in the Eastern Mediterranean Tethyan region. Lithos 65, 1–67.

Robertson, A.H.F., Dixon, J.E., 1984. Aspects of the geological evolution of the Eastern Mediterranean. In: Dixon, J.E., Robertson, A.H.F. (Eds.), The Geological Evolution of Eastern Mediterranean Geological Society of London Special Publication, pp. 1–75.

Sengör, A.M.C., Yýlmaz, Y., 1981. Tethyan evolution of Turkey: a plate tectonic approach. Tectonophysics 75, 181–241.

Sengör, A.M.C., Yýlmaz, Y., Sungurlu, O., 1984. Tectonics of the Mediterranean Cimmerides: nature and evolution of the western termination of Paleo-Tethys. In: Dixon, J.E., Robertson, A.H.F. (Eds.), Peritethyan Rift/Wrench Basins and Passive Margins Bulletin du Musée National d'histoire Naturelle, Paris, IGCP 369.

Shervais, W.J., 1982. Ti–V plots and the petrogenesis of modern and ophiolitic lavas. Earth and Planetary Science Letters 59, 102–118.

Smelik, E.A., Nyman, M.W., Veblen, D.R., 1990. Exsolution within the calcic amphibole series: natural evidence for a miscibility gap between actinolite and hornblende. Geological Society of America, Abstracts with Programs 22, A216.

Spear, F.S., 1993. Metamorphic phase equilibria and pressure–temperature–time paths. Mineralogical Society of America Monograph 1993, 799.

Stampfli, G., 2000. Tethyan oceans. In: Bozkurt, E., Winchester, J.A., Piper, J.D. (Eds.), Tectonics and Magmatism in Turkey and Surrounding Area Geological Society of London Special Publication, pp. 1–23.

Sun, S., McDonough, W.F., 1989. Chemical and isotopic systematics of oceanic basalts: Implications for mantle composition and processes. In: Saunders, A.D., Norry, M.J. (Eds.), Magmatism in the Oceans Basins. Geological Society of London Special Publication 1989 pp.313–345.

Tekeli, O., 1981. Subduction complex of pre-Jurassic age, northern Anatolia, Turkey. Geology 9, 68–72.

Thuizat, R., Whitechurch, H., Montigny, R., Juteau, T., 1981. K–Ar dating of some infra-ophiolitic metamorphic soles from the eastern Mediterranean: new evidence for oceanic thrusting before obduction. Earth and Planetary Science Letters 52, 302–310.

Vrielynck, B., Bonneau, M., Danelian, T., Cadet, J.P., Poisson, A., 2003. New insights on the Antalya nappes in the apex of the Isparta Angle: Isparta Çay unit revisited. Geological Journal 38, 283–293.

White, W.M., Tapia, M.D.M., Schilling, J.G., 1979. The petrology and geochemistry of the Azores islands. Contributions to Mineralogy and Petrology 69, 201–213.

Winchester, J.A., Floyd, P.A., 1977. Geochemical discrimination of different magma series and their differentiation products using immobile elements. Chemical Geology 16, 325–343.